Non-apoptotic caspase activity sustains proliferation and differentiation of ovarian somatic cells by modulating Hedgehog-signalling and autophagy.

Alessia Galasso[1], Daria Iakovleva[1], Luis Alberto Baena-Lopez[1]*

* Author for correspondence

1: Sir William Dunn School of Pathology. University of Oxford. South Parks Road. Oxfordshire, UK. OX13RE

Key words:

Caspases, non-apoptotic, Hedgehog-signalling, Autophagy, Patched, ovarian somatic cells.

ABSTRACT

There is increasing evidence associating the activity of caspases with the regulation of basic cellular functions beyond apoptosis. Accordingly, the dysregulation of these novel non-apoptotic functions often sits at the origin of neurological disorders, metabolic defects, autoimmunity, and cancer. However, the molecular interplay between caspases and the signalling networks active in non-apoptotic cellular scenarios remains largely unknown. Our experiments show that non-apoptotic caspase activation is critical to modulate Hedgehog-signalling and autophagy in ovarian somatic cells from both *Drosophila* and humans under moderate stress. We also demonstrate that these novel caspase functions are key to sustain stem cell proliferation and differentiation without inducing apoptosis. Finally, we molecularly link these caspase-dependent effects to the fine-tuning of the Hedgehog-receptor, Patched. Together, these findings confer a pro-survival role to the caspases, as opposed to the widely held apoptotic function assigned to these enzymes for many years.

MAIN

In recent years, expanding evidence is indicating the ability of caspases to regulate essential cellular functions beyond apoptosis (Aram et al., 2017; Baena-Lopez, 2018; Bell and Megeney, 2017; Burgon and Megeney, 2017). Accordingly, these novel non-apoptotic caspase roles ensure tissue homeostasis, whilst preventing diseases (Mukherjee and Williams, 2017). However, the molecular characterisation of these alternative caspase functions remains largely unknown in the vast majority of cell types, including stem cells. During the last decade, the investigations using the adult *Drosophila* ovary have illuminated fundamental principles of stem cell physiology and intercellular communication (Kirilly and Xie, 2007; Losick et al., 2011). Interestingly, these progenitor cells and their progeny can activate caspases at sublethal levels in response to robust environmental stress (Tang et al., 2015). Therefore, it is an ideal cellular system to study the interplay between caspases, signalling mechanisms, and stem cell physiology.

The early development of *Drosophila* female gametes occurs in a cellular structure referred to as the germarium. The germarium is formed by the germline and the surrounding somatic cells (Kirilly and Xie, 2007; Losick et al., 2011) (Figure 1A). The cellular properties within the germarium are strongly defined by the Hedgehog-signalling pathway (Chang et al., 2013; Huang and Kalderon, 2014; Huang et al., 2017; Rojas-Rios et al., 2012; Sahai-Hernandez and Nystul, 2013; Vied and Kalderon, 2009; Zhang and Kalderon, 2001). The interaction of the Hedgehog (Hh) ligand with its membrane receptor Patched (Ptc) allows the activation of the signalling transducer Smoothened (Smo) (Briscoe and Therond, 2013). This prevents the proteolytic processing of the transcriptional regulator Cubitus interruptus (Ci) (Briscoe and Therond, 2013), thus eliciting the activation of tissue-specific target genes (Briscoe and Therond, 2013). The main somatic Hh-receiving cells in the germarium are the escort cells (Rojas-Rios et al., 2012) and the follicular stem cells (Sahai-Hernandez and Nystul, 2013) (Figure 1A). As opposed to Hh-signalling deprivation (Huang and Kalderon, 2014; Sahai-Hernandez and Nystul, 2013; Zhang and Kalderon, 2001), the overactivation of Hh-pathway facilitates cell proliferation and cell differentiation in the follicular stem cells and their progeny (Chang et al., 2013; Dai et al., 2017; Singh et al., 2018; Zhang and Kalderon, 2001). Beyond the developmental requirements, Hh-signalling also prevents the excess of Ptc-induced autophagy under stress conditions, thus ensuring the homeostasis of ovarian somatic cells (Hartman et al., 2013; Singh et al., 2018). Importantly, the pro-

proliferative and differentiating roles of Hh-pathway are largely conserved in human ovarian cells with somatic origin (Li et al., 2016; Ray et al., 2011; Rosales-Nieves and Gonzalez-Reyes, 2014; Szkandera et al., 2013; Zeng et al., 2017).

In this manuscript, we establish that the cellular properties of ovarian somatic cells under moderate stress conditions are strongly influenced by the non-apoptotic caspase-dependent regulation of Hh-signalling and autophagy. At the molecular level, we connect this novel caspase functions with the fine-tuning of the Hh receptor, Ptc. In parallel, we provide preliminary evidence suggesting that our findings from *Drosophila* could be highly relevant in human cells with a comparable origin. Together, our observations uncover unknown features of stem cell regulation and caspase biology, whilst conferring a pro-survival role to these formerly pro-apoptotic enzymes.

RESULTS

There is non-apoptotic activation of *Dronc* in ovarian somatic stem cells

We recently generated a novel caspase sensor based on a cleavable, but catalytically inactive version of the effector caspase, *Drice* (Drice based sensor QF; DBS-S-QF) (Baena-Lopez et al., 2018). Amongst other applications, our reporter can provide a historical perspective of initiator caspase activation in complex *Drosophila* tissues by inducing the expression of multiple fluorescent markers with variable durability (Baena-Lopez et al., 2018) (Figure S1A). Since strong environmental stress (starvation and cold shock) can induce widespread non-apoptotic activation of effector caspases in the *Drosophila* ovary (Tang et al., 2015), we sought to investigate in detail with our sensor the features of such caspase activation under moderate stress. The detailed inspection of adult flies kept at 29^{o}C confirmed the presence of initiator caspase activation in subsets of somatic cells of the germarium (red and GFP signals, Figure 1B). Intriguingly, these cells often only displayed the fluorescent signature linked to caspase activation in the past (sensor-labelled cells in green with GFP), without signs of ongoing caspase activity (sensor-labelled cells in red with Tomato-HA) or apoptotic cell death (e.g. reporter-positive cells but TUNEL negative that did not show DNA fragmentation; Figure1B). Confirming the healthy and even proliferative status of sensor-labelled cells, we also recovered large groups of escort and follicular cells permanently decorated with the long-lasting marker induced by DBS-S-QF (lacZ positive cells, Figure 1C). Furthermore, the number of enduringly labelled germaria with this permanent caspase-tracing system increased

from 8% to 22% by comparing ovaries dissected at 7 and 14 days after adult eclosion, respectively (Figure 1D). These results show for the first time the presence of transient and non-apoptotic activation of initiator caspases under moderate stress in somatic cells of the germarium, including the proliferative stem cell precursors.

Since DBS-S-QF was specifically designed to report on the activity of initiator caspases (mainly *Dronc*, the *Drosophila* orthologue of the mammalian caspase-2/9), we sought to investigate the transcriptional regulation of *Dronc* in the ovary using a *Dronc*$^{KO\text{-}Gal4}$ line that recapitulates its physiological expression (Arthurton et al., 2019). Interestingly, *Dronc*$^{KO\text{-}Gal4}$ induced the expression of a neutral cellular marker (Histone-RFP) in variable subsets of escort and follicular cells in the germarium, as well as the polar and stalk cells (Figures 1E, 1F, and S1B). Subsequent cell lineage-tracing experiments confirmed this pattern of expression (Figure S1C). Next, we assessed whether this transcriptional regulation led to accumulating Dronc as a protein. To that end, we used a *Dronc* allele endogenously tagged with the biotin ligase TurboID (Shinoda et al., 2019). The TurboID allows the detection of low protein level concentrations through the biotinylation of peptides in close proximity to the TurboID-tagged protein (Shinoda et al., 2019). In line with our previous data, all of the cell types transcriptionally upregulating *Dronc* showed a consistent biotinylation enrichment (Figures 1G, and S1D). Confirming the specificity of the TurboID labelling, a version of Drice fused to the TurboID (Shinoda et al., 2019) generated an equivalent labelling of the follicular cells but no biotinylation enrichment was detected in stalk cells, and the signal was noticeably weaker in the germline (Figure S1E). Together, our results establish that there is enriched expression and transient non-apoptotic activation of Dronc in follicular stem cells of the germarium and their progeny under moderate stress conditions.

***Dronc* acts as a pro-survival factor that sustains follicular stem cell functions.** To determine the biological significance of Dronc activation in the germarium, we generated morphogenetic mosaics using a *Dronc*^{I29} null allele. These genetic mosaics only caused morphological alterations and differentiation defects in the follicular cells (Castor downregulation) when *Dronc* expression was eliminated in large clones that encompassed the presumptive follicular stem cells (compare Figure S1F with S1G). However, these clones appeared with very low frequency (11,4% (4/35); total number of clones analysed n=35 in 85 germaria) after applying a well-established experimental regime of repetitive heat-shocks (Laws and Drummond-Barbosa, 2015) that defeated our purpose to investigate the functional requirement of

Dronc under moderate stress. More importantly, the clones with associated phenotypes usually showed the expression of *Dronc* compromised in both the somatic cells and germline, thus preventing us to extract unambiguous conclusions. To circumvent these technical limitations, we took advantage of a conditional null allele of *Dronc* generated in the laboratory through genome engineering (Arthurton et al., 2019; Baena-Lopez et al., 2013). This allele contains a wild-type *Dronc* cDNA flanked by FRT recombination sites (Figure S1H). After Flippase-mediated recombination, the permanent excision from the genome of FRT-rescue cassette can efficiently convert wild type cells into mutant (Arthurton et al., 2019; Baena-Lopez et al., 2013). Importantly, this allele conversion process does not require extreme heat-shock treatments and it can reproducibly be induced with temporal and spatial precision in specific cell populations by combining the *flippase* recombinase with the Gal4/UAS gene expression system (Brand and Perrimon, 1993). Downstream of the FRT-rescue cassette, we placed a transcriptional activator QF (Riabinina and Potter, 2016), which facilitates the expression of any gene of interest under the physiological regulation of *Dronc* (hereafter $Dronc^{FRT\text{-}Dronc\text{-}FRT\text{-}QF}$, Figure S1H) (Arthurton et al., 2019). Capitalising on these features and using the *109-30*-Gal4 driver, we reproducibly eliminated the expression of *Dronc* from the follicular stem cells and their progeny (Sahai-Hernandez and Nystul, 2013) (Figure S2A-C). Validating our experimental approach, all of the inspected germaria (100%, n=14) showed GFP signal (QUAS-*GFP*) in the follicular stem cells and their progeny (follicular cells and a subset of contiguous escort cells; Figure S2D). More importantly, this genetic manipulation significantly reduced the total number of follicular cells of the germarium, and the proportion of follicular cells expressing the follicular differentiation marker Castor (Figures 2A-C and S2C). Expectedly, the concomitant elimination of *Dronc* expression in escort and follicular cells, using the *ptc*-Gal4 (Figures S2E-H), caused equivalent defects (reduced cell number and Castor downregulation; Figures 2C and S2E-H). To determine whether these phenotypes were due to proliferation defects, we next analysed the cell cycle profile of follicular cells with the marker termed Fly-Fucci (Zielke et al., 2014). This analysis revealed an increased proportion of follicular cells in S-phase at expense of cells in G0 in *Dronc* mutant conditions (Figure 2D-F). These results were confirmed by assessing the incorporation of the S-phase marker EdU in follicular cells mutant for *Dronc* (Figure 2G). Since the accumulation of follicular cells in S-phase did not lead to an excess of follicular cells but a reduction (Figure 2C) and did not alter other stages of the cell cycle (Figure 2F), we rationalised that *Dronc* mutant follicular cells have a slow transition through this cell cycle stage that compromises their proliferation rate.

Discarding a relevant contribution of cell death to our phenotypes, we also noticed that the number of TUNEL-positive follicular cells both in wildtype and *Dronc*-mutant conditions was comparable (Figure S2I). Complementarily, the overexpression of *Dronc* also failed to cause excess apoptosis in our experimental conditions (Figure S2I). To complete this set of experiments, we confirmed the specificity of the phenotypes generated by the QF allele replacing this element with a Suntag-HA-Cherry peptide (*Dronc*$^{\text{FRT-Dronc-FRT-suntag-HA-cherry}}$) (Arthurton et al., 2019) (Figures S1H and 2H). This new allele conversion mimicked the follicular defects previously obtained with the QF construct (compare Figure 2C with 2H). Collectively, these results indicated that non-apoptotic activation of *Dronc* stimulates the proliferation and differentiation of follicular stem cells and their progeny under moderate stress conditions.

The pro-survival effects of Dronc demands its catalytic activity

Most functions of caspases rely on their enzymatic activity post activation, but some of the non-apoptotic roles only demand protein-protein interactions (Napoletano et al., 2017; Ouyang et al., 2011). To investigate the molecular activities of *Dronc* required in follicular cells, we used a different conditional allele that contains after the rescue- cassette a mutant form of *Dronc* with two mutations, C318A and E352A (*Dronc*$^{\text{FRT-Dronc-FRT-FLCAEA}}$; Figure S1H (Arthurton et al., 2019)). These mutations prevent the enzymatic function and proteolytic activation of *Dronc*, respectively (Chai et al., 2003; Muro et al., 2004). This allele (*Dronc*$^{\text{FRT-Dronc-FRT-FLCAEA}}$) caused a comparable reduction in the number of follicular cells and Castor expression defects to that previously observed with other *Dronc* alelles (Figure 2H). These results strongly suggested an enzymatic requirement of *Dronc* in follicular cells. To validate this hypothesis, we next investigated the potential implication of the primary *Dronc* substrates in our cellular model; the so-called effector caspases (drICE, DCP-1, Decay and Damm) (Leulier et al., 2006). To avoid the functional redundancy between these caspase members (Xu et al., 2006), we simultaneously targeted their expression in follicular cells by combining validated UAS-RNAi transgenes (Leulier et al., 2006) with the *109-30*-Gal4 driver. These experiments replicated the results obtained eliminating the expression of *Dronc* (Figure 2H). Furthermore, the overexpression in somatic cells of the effector caspase inhibitor P35 (Hay et al., 1994) also mimicked the proliferation and differentiation defects of follicular cells (Figure 2H). These findings indicate that the non-apoptotic activation of the caspase

pathway provides pro-survival cues that sustain the proliferation and differentiation of the follicular cells under moderate stress.

Caspase activation promotes Hh-signalling acting upstream of *smoothened*

Hh-signalling deficiency in follicular stem cells causes phenotypes highly reminiscent to that of *Dronc* mutant conditions (Huang and Kalderon, 2014; Huang et al., 2017) (Figures 3A-C). Therefore, we investigated the activation levels of this pathway in *Dronc* mutant cells. *Dronc* insufficiency in somatic cells reduced the expression levels of the active form of Cubitus interruptus (Ci-155 (Motzny and Holmgren, 1995), Gli in mammals), as well as the transcription of the universal Hh-target gene, *ptc* (Briscoe and Therond, 2013) (Figure 3A-C). Importantly, similar Hh-signalling defects were detected in human ovarian cells with somatic origin (OVCAR-3) deficient in *caspase-9* (Figure 3D and 3E). A previously validated set of primers was used to estimate the transcriptional levels of *patch1* through qPCR in this set of experiments (Liao et al., 2009). To functionally confirm the crosstalk between caspases and Hh-signalling, we attempted to rescue the *Dronc* mutant phenotypes by overexpressing either a constitutively active form of *smoothened* (*smo*) or Ci. The invidual overexpression of these Hh-components restored the proliferation and Castor expression defects caused by the *Dronc* insufficiency (Figures 3F-H, S3D, and S3E). Together, these data strongly suggested a crosstalk between caspases and Hh-pathway in ovarian somatic cells.

Since we rescued the mutant phenotypes of *Dronc* by either expressing an active form of Smo or Ci, we rationalised that the intersection of *Dronc* with the Hh-pathway might occur upstream of *smo*. To test this possibility, we performed classical genetic epistasis between *Dronc* and *ptc*. Intriguingly, we noticed that Castor expression was downregulated in double heterozygous mutant follicular cells (*ptc*-Gal4/+; $Dronc^{KO}$ /+) (Figure S4A; notice that the Gal4 line was generated by a random insertion of a P-element in the regulatory region of *ptc* that created a weak hypomorh allele (Shyamala and Bhat, 2002)). Furthermore, these differentiation defects were correlated with lower levels of Hh-signalling, as indicated by the downregulation of *ptc*-GFP (compare Figure 3A with Figure S4A; notice that *ptc*-GFP is also a *ptc* hypomorph allele (Buszczak et al., 2007)) and Ci-155 (compare Figure S4A and

S4B). Confirming the legitimate nature of the potential genetic interaction between *ptc* and *Dronc*, Castor was also downregulated in ovarian somatic cells expressing a *Dronc*-RNAi construct, as well as in double heterozygous flies combining null alleles for ptc^{S2} and $Dronc^{KO}$ (ptc^{S2}/+; $Dronc^{KO}$/+) (Figure S4C and 4D). On the contrary, the overexpression of a wild type form of *Dronc* rescued the Castor expression defects of double heterozygous *ptc*-Gal4:$Dronc^{KO}$ germaria (Figure 3I). Furthermore, we noticed that the proliferation phenotypes were *Dronc* dose-dependent and separable from the differentiation defects, since they only appeared in *Dronc*-mutant homozygous conditions (compare Figure 2C with 3I). Together, these experiments confirmed a *bona fide* but initially counterintuitive genetic interaction between *ptc* and *Dronc*. Because Ptc is the receptor of Hh but acts as a negative regulator in terms of signalling, one would predict the functional rescue of *Dronc* deficiency after reducing *ptc* expression. Instead, the mild double insufficiency of *ptc-Dronc* generated phenotypes highly reminiscent to Hh-signalling defects or *Dronc* deprivation (compare Figure 3I with S3A-C, and Figure 2C).

Dronc regulates Hh-signalling through the fine-tuning of Ptc

To better understand at the molecular level the interplay between *Dronc* and *ptc*, we investigated the Ptc protein levels within *Dronc* mutant somatic cells. Although *ptc* was transcriptionally downregulated in *Dronc* mutant conditions (Figures 3A-C and Figure S4A), the protein levels were strikingly elevated within escort and follicular cells in *Dronc* conditions (Figures 4A-C). Furthermore, the Ptc-positive punctae were significantly enlarged in *Dronc*-deficient cells (Figure Suppl.4E). Importantly, similar aggregates were observed overexpressing a mutant form of Ptc^{1130X} that is highly stable at the plasma membrane and therefore shows low rates of degradation (Lu et al., 2006) (Figure S4F-H). To assess functionally the biological significance of Ptc aggregates, we reduce the levels of Ptc in *Dronc* mutant cells by either expressing a Ptc-RNAi construct or using a stronger hypomorph combination for *ptc*. Both genetic manipulations largely restored the expression of Castor in *ptc-Dronc* double heterozygous germaria (Figures 4D and Figure S4I). These results suggested that *Dronc* takes part in the molecular network that regulates the fine-tuning of Ptc in ovarian somatic cells. Moreover, the accumulation of Ptc in caspase-deficient cells is largely responsible for the Hh-signalling deprivation, and ultimately the phenotypes in follicular cells.

Dronc differentiation phenotypes are partially linked to Ptc-induced autophagy

Beyond the Hh-regulatory role, it has recently been reported the ability of Ptc to induce autophagy in ovarian somatic cells from *Drosophila* and mammals (Jimenez-Sanchez et al., 2012; Singh et al., 2018). Therefore, we sought to assess whether Ptc aggregates within *Dronc* mutant cells were able to induce this cellular process. To assess the autophagy flux in the germarium, we used the expression of Ref2P (the *Drosophila* ortholog of the mammalian p62 (Nezis et al., 2008)). Whereas the activation of autophagy reduces the intracellular levels of Ref2P/p62, its inhibition facilitates Ref2P/p62 accumulation (Bjorkoy et al., 2009). In agreement with the previous literature (Jimenez-Sanchez et al., 2012; Singh et al., 2018), the expression of Ref2P increased in a genetic condition that modestly reduced Ptc protein levels (*ptc*-Gal4/+) (Figures 5A-C). However, this upregulation was prevented by reducing the dosage of *Dronc* (*ptc*-Gal4/+; $Dronc^{KO}$ /+) (Figures 5A-C). These results suggested an increased autophagy flux in *Dronc* mutant conditions. To evaluate functionally the potential contribution of this cellular process to the *Dronc* phenotypes, we blocked the early steps of autophagy by expressing an *Atg1*-RNAi construct with demonstrated activity in the *Drosophila* ovary (Rojas-Rios et al., 2015). The lack of autophagy linked to this genetic manipulation partially rescued the Castor expression in a *ptc-Dronc* mutant background (Figure 5D). These findings indicated that the non-apoptotic activation of *Dronc* modulates the intracellular levels of Ptc, which subsequently determine the fine-tuning of Hh-pathway and autophagy. Furthermore, they showed that the differentiation phenotypes induced by *Dronc* deficiency are critically linked with the *Ptc*-dependent activation of autophagy. Next, we investigated the potential conservation of the *Drosophila* autophagy-related findings in human OVCAR-3 cells. Although the protein levels of p62 remained unaltered in *Caspase-9* mutant cells in standard culture conditions (Figures 5E and 5F), they were significantly reduced after adding low concentrations of EtOH (Figures 5E and 5F). Importantly, previous reports have shown that low levels of EtOH can trigger moderate cellular stress and activation of autophagy (Li et al., 2014). Confirming the specificity of p62 downregulation in our experiments, the inhibition of autophagy with bafilomycin (Mauvezin and Neufeld, 2015) restored the expression levels of p62 in *Caspase-9* deficient cells treated with EtOH (Figure 5E-F). These findings preliminarily suggest that the regulatory role of caspases on Hh-signalling and autophagy under moderate stress could be relevant in human cellular settings.

DISCUSSION

Although caspases have traditionally been studied as main drivers of apoptosis, recent findings are implicating these enzymes in the regulation of basic cellular functions independent of apoptosis. However, complete understanding of such functions remains elusive in most cellular settings, including stem cells. Our findings provide solid evidence indicating that the non-apoptotic activation of the caspase-pathway is key to sustain Hh-signalling and prevent autophagy in ovarian somatic cells under moderate stress conditions. Furthermore, we have shown that these unexpected caspases functions play a pro-survival role that ensures the proliferation and differentiation of ovarian somatic cells. These findings shed light on unknown aspects of caspase biology that interestingly could also be relevant in human cells.

Non-apoptotic activation of Dronc acts as a pro-survival factor in ovarian somatic stem cells

Our experiments have shown the widespread expression and activation of caspases in *Drosophila* ovarian somatic cells without causing apoptosis (Figure 1 and Figure S1). Confirming the non-apoptotic nature of such caspase activation, caspase deficiency compromises the cell proliferation and differentiation of follicular stem cells and their progeny (Figure 2). Furthermore, we show that these novel non-apoptotic functions can molecularly be linked to the caspase-dependent regulation of Hh-signalling and autophagy. Together, these findings caution against the generic association of non-apoptotic patterns of caspase activation with the phenomenon of anastasis (pure recovery of caspase-activating cells from the “brink of death”) (Ding et al., 2016; Sun et al., 2017). Alternatively, they suggest that non-apoptotic caspase activation could be essential for regulating cell signalling and pro-survival functions independently of apoptosis (Aram et al., 2017; Baena-Lopez, 2018; Bell and Megeney, 2017; Burgon and Megeney, 2017).

Molecular basis of the caspase-dependent regulation of Hh-signalling and autophagy

At the molecular level, we provide evidence that non-apoptotic activation of Dronc prevents the accumulation of Ptc receptor (Figure 4). Since Ptc accumulation is not correlated with its transcriptional upregulation (Figure 3), we conclude that caspase activation likely enhances the degradation rate of Ptc. Supporting this hypothesis, a mutant form of Ptc^{1130X} largely stable in the plasma membrane (Lu et al., 2006) also accumulates in large punctae in *Dronc*-mutant ovarian somatic cells (Figures S4F-H). However, two factors strongly argue against the possibility that *Dronc* directly

facilitates the degradation of Ptc through proteolytic processing. First, the relevant targets implementing the functions of *Dronc* in somatic cells appear to be the so-called effector caspases (Figure 2H). Second, the interplay between *Dronc* and *ptc* appears to be highly specific to the *Drosophila* germarium, whereas caspases and Ptc coexist in many other *Drosophila* tissues. An alternative explanation to the effects of caspases on Ptc could be a potential regulatory action of caspases on the ubiquitin ligases involved in Ptc degradation. Interestingly, specific ubiquitin ligases have been shown to physically interact and activate Caspase-9 in mammalian cells deprived of Hh-signalling (Fombonne et al., 2012; Mille et al., 2009). However, the direct connection of our caspase functions with Smurf (the ubiquitin ligase ortholog in *Drosophila* (Li et al., 2018)) also seems unlikely. In contrast to *Dronc* phenotypes, the function of *smurf* is not restricted to the ovary (Liang et al., 2003). Additionally, if caspases would mediate the proteolytic degradation of Smurf, the excess of this protein in caspase mutant cells should reduce the Ptc levels (Li et al., 2018) but instead, Ptc is significantly accumulated in caspase mutant conditions. Although further experiments out of the scope of this manuscript are needed to fully understand the molecular details of the relation between caspases and Ptc, our findings establish a novel functional connection between these two molecular factors in a complex cellular setting, which in turn modulates the implementation of essential cellular functions.

Beyond repressing Hh-signalling, the accumulation of Ptc in *Dronc* mutant follicular cells can induce autophagy (Jimenez-Sanchez et al., 2012; Singh et al., 2018) (Figure 5). Furthermore, this activation of autophagy contributes to the differentiation defects observed in *Dronc* mutant conditions (Figure 5). Previous studies have associated *Dronc* with the regulation of autophagy (Daish et al., 2004; Martin and Baehrecke, 2004); however, our data establish unprecedented links between this cellular process, Hh-pathway, and the caspases. Interestingly, as shown in *Drosophila* cells, *caspase-9* deficiency appears to dysregulate Hh-signalling (Figure 3) and autophagy (Figure 5) in human ovarian cells under moderate stress. To some extent, these results preliminarily suggest that caspases could be part of an evolutionarily conserved genetic network able to modulate Hh-signalling and autophagy in ovarian somatic cells (Figure 5G).

Cellular, physiological and evolutionary implications of non-apoptotic caspase activation in ovarian somatic cells

At the cellular level, caspase deficiency causes proliferation and differentiation defects in *Drosophila* ovarian somatic cells under stress. The proliferation phenotypes are likely correlated with Hh-signalling since solid evidence indicates the implication of this pathway in the regulation of the cell cycle (Agathocleous et al., 2007; Roy and Ingham, 2002). Supporting this hypothesis, we have shown that the proliferation phenotypes disappear after restoring Hh-signalling in caspase mutant follicular cells (Figure 3H). Interestingly, caspase-dependent proliferation and differentiation phenotypes are separable and demand different levels of caspase activation. Whereas the downregulation of Castor appears in *ptc-Dronc* heterozygous cells (Figure 3I), the proliferation defects only emerge in *Dronc* homozygous conditions (compare Figure 2C with 3I). Furthermore, the expression of Castor can be largely restored by preventing the excess of autophagy in *ptc-Dronc* heterozygous cells (Figure 5D). These data suggest that the differentiation phenotypes are strongly linked with the excess of autophagy; however, the downregulation of Castor is not directly responsible for the proliferation defects (Figure 5G). Furthermore, they confirm the non-apoptotic nature of the caspase activation in our experimental conditions, since the differentiation defects are not associated with the reduction in the number of follicular cells. More importantly, they indicate that even though sustained caspase activation due to persistent signalling defects and/or environmental stress can lead to apoptosis (Fadeel and Orrenius, 2005), non-apoptotic levels of caspase activation could be at the forefront of the cell survival mechanisms against cellular stress in ovarian somatic cells (Figure 5G). This dual role of caspases coupled to different signalling pathways and cellular contexts could be an effective mechanism to ensure tissue homeostasis and/or to trigger cellular selection processes in multiple cellular scenarios (Moreno et al., 2002).

From a physiological perspective, it is has been reported that Hh-downregulation triggered by environmental stress restricts egg laying and promotes autophagy in *Drosophila* (Huey et al., 1995; Terashima and Bownes, 2004; Terashima et al., 2005). Similarly, Hh deregulation and/or exacerbated autophagy can compromise follicular development in mammalian systems (Pepling, 2012; Zhou et al., 2019). Our work suggests that sublethal caspase activation influences Hh-signalling and autophagy (Figure 5G), and therefore it might be part of a complex adaptive system that ensures timely egg maturation in stress situations.

Taking into consideration the non-apoptotic roles of ancient members of the caspase family (Bell and Megeney, 2017; Dick and Megeney, 2013; Lee et al., 2010), our

findings may also have evolutionary implications. Since Dronc can play a pro-survival role in somatic cells, our data support the hypothesis that caspases could initially sustain basic cellular processes, and only their inadvertent/persistent activation would lead to cell death (Dick and Megeney, 2013). From this perspective, these pro-apoptotic enzymes could act as pro-survival factors, thus inverting the widely held view regarding their most primitive function.

MATERIAL AND METHODS

Fly Strains and fly husbandry details

All fly strains used are described at www.flybase.bio.indiana.edu unless otherwise indicated. After 24h of egg laying at 25°C, experimental specimens were raised at 18°C, thus enabling the repression of Gal4 activity through a Gal80^{ts}. This prevents lethality in our experiments during larval and pupal stages. After hatching, adults were then transferred from 18°C to 29°C until dissection time. At 29°C the repression of Gal80^{ts} disappears, and therefore gene expression via Gal4 is elicited within specific cell subpopulations of the germarium. The temperature shift of adult flies at 29°C was also maintained for those genetic combinations that were not lethal in previous developmental stages.

Genotypes

Full description of experimental genotypes appearing in each figure.

Figure 1

1B. Actin *DBS-S-QF*, UAS-*mCD8-GFP*, QUAS-*tomato-HA*/+;; QUAS-*Gal4*/+

1C and **1D**. Actin *DBS-S-QF*, UAS-*mCD8-GFP*, QUAS-*tomato-HA*/+; QUAS-*flippase* (BL30126)/+; Actin5C FRT-*stop*-FRT *lacZ*-nls/+ (BL6355)

1F. w;; *Dronc*$^{KO\text{-}Gal4}$ / UAS-*Histone-RFP* (BL56555)

1G. w;; *Dronc*^{TurboID} (a gift from Masayuki Miura)/ Tm3, Sb

Figure 2

2A: *109-30-Gal4* (BL7023)/+; *Dronc*^{KO} Tub-*G80*^{ts} (BL7019)/+;

2B: *109-30-Gal4* (BL7023)/+; *Dronc*^{KO} Tub-*G80*^{ts} (BL7019)/ UAS-*flippase* (BL8209) *Dronc*$^{KO\text{-}FRT\text{-}Dronc\text{-}GFP\text{-}APEX\text{-}FRT\text{-}QF}$.

2C. From left to right:

CTRL= 109-30-Gal4 (BL7023)/+; *Dronc*^{KO} Tub-*G80*^{ts} (BL7019)/+;

Dronc -/- = 109-30-Gal4 (BL7023)/+; *Dronc*^{KO} Tub-*G80*^{ts} (BL7019)/ UAS-*flippase* (BL8209) *Dronc*$^{KO\text{-}FRT\text{-}Dronc\text{-}GFP\text{-}APEX\text{-}FRT\text{-}QF}$.

CTRL=ptc-Gal4 (BL2017)/+; +/+

Dronc -/- = ptc-Gal4 (BL2017)/+; *Dronc*^{KO} Tub-*G80*^{ts} (BL7019)/ UAS-*flippase* (BL8209) Dronc$^{KO\text{-}FRT\text{-}Dronc\text{-}GFP\text{-}APEX\text{-}FRT\text{-}QF}$.

2D. *109-30-Gal4* (BL7023)/FUCCI(BL55123); *Dronc*^{KO} Tub-*G80*^{ts} (BL7019)/ +

2E. *109-30-Gal4* (BL7023)/FUCCI(BL55123); *Dronc*^{KO} Tub-*G80*^{ts} (BL7019) / UAS-*flippase* (BL8209) *Dronc*$^{KO\text{-}FRT\text{-}Dronc\text{-}GFP\text{-}APEX\text{-}FRT\text{-}QF}$.

2F. From left to right:

CTRL= 109-30-Gal4 (BL7023)/FUCCI(BL55123); *Dronc*^{KO} Tub-*G80*^{ts} (BL7019)/ +

Dronc -/- = 109-30-Gal4 (BL7023)/FUCCI(BL55123); *Dronc*^{KO} Tub-*G80*^{ts} (BL7019) / UAS-*flippase* (BL8209) *Dronc*$^{KO\text{-}FRT\text{-}Dronc\text{-}GFP\text{-}APEX\text{-}FRT\text{-}QF}$.

2G. From left to right:

CTRL= ptc-Gal4 (BL2017)/+; Tub-*G80*^{ts} (BL7019)/+

Dronc -/- = ptc-Gal4 (BL2017)/+; *Dronc*^{KO} Tub-*G80*^{ts} (BL7019) / UAS-*flippase* (BL8209) *Dronc*$^{KO\text{-}FRT\text{-}Dronc\text{-}GFP\text{-}APEX\text{-}FRT\text{-}QF}$.

2H. From left to right:

Dronc Suntag = 109-30-Gal4 (BL7023)/+; *Dronc*^{KO} Tub-*G80*^{ts} (BL7019) / UAS-*flippase* (BL8209) *Dronc*$^{KO\text{-}FRT\ Dronc\text{-}GFP\text{-}Apex\ FRT\text{-}Suntag\text{-}HA\text{-}Cherry}$

Dronc FLCAEA= 109-30-Gal4 (BL7023)/+; *Dronc*^{KO} Tub-*G80*^{ts} (BL7019) / UAS-*flippase* (BL8209) *Dronc*$^{KO\text{-}FRT\ Dronc\text{-}GFP\text{-}Apex\ FRT\text{-}Dronc\ FL\text{-}CAEA\text{-}Suntag\text{-}HA\text{-}Cherry}$

Eff. Casp. RNAi = 109-30-Gal4 (BL7023)/UAS-*Drice*RNAi UAS-*Decay*RNAi (a gift from Pascal Meier); UAS-*Damm*RNAi, UAS-*Dcp1*RNAi (a gift from Pascal Meier).

2x P35 = ptc-Gal4 (BL2017)/UAS-P35 (BL5072); UAS-P35 (BL5073)/+

Figure 3

3A. *109-30-Gal4* (BL7023)*/ptc*-GFP^{CB02030} (a gift from Isabel Guerrero). *ptc*-GFP^{CB02030} contains a P-element insertion in the promoter region of *ptc* that generates a weak hypomorph allele of *ptc*(Buszczak et al., 2007).

3B.*109-30-Gal4* (BL7023)*/ptc*-GFP^{CB02030}*; Dronc*^{KO}Tub-*G80*^{ts} (BL7019)/ UAS-*flippase* *Dronc*$^{KO\text{-}FRT\text{-}Dronc\text{-}GFP\text{-}APEX\text{-}FRT\text{-}QF}$

3F. *109-30-Gal4* (BL7023)/UAS-*smo*^{Act} (BL44621); *Dronc*^{KO}Tub-*G80*^{ts} (BL7019)/+

3G.*109-30-Gal4* (BL7023)/UAS-*smo*^{Act} (BL44621); *Dronc*^{KO}Tub-*G80*^{ts} (BL7019)/ UAS-*flippase* (BL8209) *Dronc*$^{KO\text{-}FRT\text{-}Dronc\text{-}GFP\text{-}APEX\text{-}FRT\text{-}QF}$

3H. From left to right:

CTRL= 109-30-Gal4 (BL7023)/UAS-*smo*^{Act} (BL44621); *Dronc*^{KO}Tub-*G80*^{ts} (BL7019)/+

Dronc -/- = 109-30-Gal4 (BL7023)/UAS-*smo*^{Act} (BL44621); *Dronc*^{KO}Tub-*G80*^{ts} (BL7019)/ UAS-*flippase* (BL8209) *Dronc*$^{KO\text{-}FRT\text{-}Dronc\text{-}GFP\text{-}APEX\text{-}FRT\text{-}QF}$

CTRL= 109-30-Gal4 (BL7023)/UAS-*Ci* (BL28984); *Dronc*^{KO}Tub-*G80*^{ts} (BL7019)/+

Dronc -/- = 109-30-Gal4 (BL7023)/UAS- UAS-*Ci* (BL28984); *Dronc*^{KO}Tub-*G80*^{ts} (BL7019)/ UAS-*flippase* (BL8209) *Dronc*$^{KO\text{-}FRT\text{-}Dronc\text{-}GFP\text{-}APEX\text{-}FRT\text{-}QF}$

3I. From left to right:

Dronc +/+ = ptc-Gal4 (BL2017)/+; Tub-*G80*^{ts} (BL7019)

Dronc +/- = ptc-Gal4 (BL2017)/+; *Dronc*^{KO}Tub-*G80*^{ts} (BL7019)/+

Dronc +/- UAS-Dronc = ptc-Gal4 (BL2017)/+; *Dronc*^{KO}Tub-*G80*^{ts} (BL7019)/UAS-*Dronc* (BL56198)

Figure 4

4A-C. From left to right:

Dronc^{KO}Tub-*G80*^{ts} (BL7019)/+

ptc-Gal4 (BL2017)/+; Tub-*G80*^{ts} (BL7019)/+

ptc-Gal4 (BL2017)/+; *Dronc*^{KO}Tub-*G80*^{ts} (BL7019)/+

4D. From left to right:

CTRL = *109-30*-Gal4 (BL7023)/+; *Dronc*^{KO}Tub-*G80*^{ts} (BL7019)/+

Dronc -/- = *109-30Gal4* (BL7023)/+; *Dronc*^{KO}Tub-*G80*^{ts} (BL7019)/ UAS-*flippase* (BL8209) *Dronc*$^{KO\text{-}FRT\text{-}Dronc\text{-}GFP\text{-}APEX\text{-}FRT\text{-}QF}$

Dronc -/- UAS-*ptc*-RNAi = *109-30Gal4* (BL7023)/UAS-*ptc*-RNAi (BL55686); *Dronc*^{KO}Tub-*G80*^{ts} (BL7019)/ UAS-*flippase* (BL8209) *Dronc*$^{KO\text{-}FRT\text{-}Dronc\text{-}GFP\text{-}APEX\text{-}FRT\text{-}QF}$

Figure 5

5A-C. From left to right:

Dronc^{KO}Tub-*G80*^{ts} (BL7019)/+

ptc-Gal4 (BL2017)/+; Tub-*G80*^{ts} (BL7019)/+

ptc-Gal4 (BL2017)/+; *Dronc*^{KO}Tub-*G80*^{ts} (BL7019)/+

5D. From left to right:

CTRL= *ptc*-Gal4 (BL2017)/+; Tub-*G80*^{ts} (BL7019)/+

Dronc +/- = *ptc*-Gal4 (BL2017)/+; *Dronc*^{KO}Tub-*G80*^{ts} (BL7019)/+

CTRL= *ptc*-Gal4 (BL2017)/+; Tub-*G80*^{ts} (BL7019)/UAS-*Atg1*-RNAi (BL35177)

Dronc +/- = *ptc*-Gal4 (BL2017)/+; *Dronc*^{KO}Tub-*G80*^{ts} (BL7019)/UAS-*Atg1*-RNAi (BL35177)

Immunohistochemistry

Adult *Drosophila* ovaries were dissected on ice-cold PBS. Immunostainings and washes were performed according to standard protocols (fixing in PBS 4% paraformaldehyde, washing in PBT 0.3% (0.3% Triton X-100 in PBS). Primary antibodies used in our experiments were: anti-Castor (1:2000; a gift from Alex Gould); rabbit anti-HA (1:1000; Cell Signaling C29F4); mouse anti-β-Gal (1:500; Promega Z378B); chicken Anti-βGal (1:200, Abcam AB9361); Anti-FasIII (1:75, Hybridoma Bank 7G10); Anti-Ci-155-full length (1:50, Hybridoma Bank 2A1); Anti-Ptc (1:50, Hybridoma Bank Apa1); Anti-Ref2P (1:300, abcam 178440). Conjugated secondary antibodies (Molecular Probes) were diluted in 0.3% PBT and used in a final concentration (1:200): conjugated donkey anti-rabbit Alexa-Fluor-488 (A21206) or 555 (A31572) or 647 (A31573), conjugated donkey anti-mouse Alexa-Fluor-488

(A21202) or 555 (A31570) or 647 (A31571), conjugated goat anti-rat Life Technologies (Paisley, UK) Alexa-Fluor- 488 (A21247) or 555 (A21434). The detection of biotinylated proteins was made using Streptavidin conjugated with the 488 fluorophore (1:500; S11223). Dapi was added to the solution with the secondary antibodies for labelling the nuclei (1:1000; Thermo Scientific 62248). Following incubation in secondary antibodies, samples were washed several times during 60 minutes in PBT. Finally, they were mounted on Poly-Prep Slides (P0425-72EA, Sigma) in Aqua-Poly/Mount (Polysciences, Inc (18606)).

TUNEL staining

Like in the immunochemistry, follicles from adult *Drosophila* females were dissected in ice-cold PBS and fixed in PBS containing 4% formaldehyde for 20'. After fixation, the samples were washed 3 times for 15' with PBS and subsequently permeabilised with PBS containing 0,3% triton and 0,1% sodium citrate for 8' on ice. 3 PBS washes for 20' with were performed also after permeabilisation. The *in situ* detection of fragmented genomic DNA was performed according to the DeadEnd colorimetric TUNEL (Terminal transferase-mediated dUTP nick-end labeling) system (Promega). Briefly, samples were first equilibrated at room temperature in equilibration buffer (5-10') and then incubated with TdT reaction mix for 1 hour at 37°C in a humidified chamber to obtain the 3'-end labelling of fragmented DNA. The reaction was terminated with 3 washes for 15' in PBS. If necessary, the TUNEL protocol was followed by standard immunofluorescent staining. The detection of TUNEL-positive cells was achieved by an incubation of 45' with streptavidin-fluorophore conjugated dyes.

EdU Staining.

Adult female ovaries were dissected in PBS1X, transferred to a microfuge tube containing 10mM EdU in PBS1X and kept at room temperature on a shaker for 1□h. Ovarioles were then dissociated, fixed, and stained with primary and secondary antibodies as described above. The EdU detection reaction was performed according to the manufacturer's manual (Thermo Fisher Scientific, C10640).

Morphogenetic mosaics generation.

Two-day old adult females of the genotype yw hs-*Flp*$^{1.22}$/+; UAS-*flippase*/+; FRT80, *Dronc*^{I29}/ FRT80 Ubiquitin-*GFP* were given either two or four 1 hour heat-shocks at 37ºC spread over 2 days (12h apart). This allowed variable mitotic recombination efficiency and therefore different number of genetic mosaics. The higher is the

number of heat-shocks, the larger is the probability of covering a large fraction of tissue with mutant cells. After the last heat shock, flies were kept at 29°C under a regime of frequent transfer (every two days) to a fresh vial with standard food supplemented with yeast. Flies were dissected and immunostained 7days after the last heat shock.

Imaging.

Drosophila ovarioles were imaged using the Olympus Fluoview FV1200 and associated software. Z-stacks were taken with a 40X objective at intervals along the apical-basal axis that ensured adequate resolution along Z-axis (step size 0.5-1.5-µm). The same confocal settings were used during the image acquisition process of experimental and control samples. Acquired images were processed using ImageJ 1.52n software(Schneider et al., 2012), Adobe Photoshop2020 and Adobe Illustrator2020 in order to complete the figure preparation.

Image quantification

All of the images used in this study were randomised and blindly scored during the quantification process. Images for quantification purposes were processed with ImageJ 1.52p.

The total number of cells in the FasIII expression domain of the germarium was counted manually using an ImageJ Cell Counter macro specifically written to that purpose (Figures 2C,2H,3H,3I,4D,5D, and Figure S3C). This macro avoids the duplicated counting of the same object through the different focal planes of the acquired image. The same procedure was followed to estimate the number of Castor expressing cells in the FasIII cellular domain of the germarium.

To quantify the number and size of Ptc and Ref2P-positive particles in the regions 1, 2a and 2b of the germarium (Figures 4B,5B, and Figure S4E), we first made a maximum projection of the total focal planes. Then we sequentially applied the thresholding and “Analyse Particles” plug-ins from ImageJ. An equivalent image processing method was used to estimate the Ptc expression levels in Figures 3C and Figure S4H. The “mean gray value” function of image J was used in this instance to estimate the GFP levels.

Western Blot

Adult *Drosophila* ovaries were dissected in ice-cold PBS and snap-frozen in liquid nitrogen. Subsequently, they were homogenised in NP40 buffer [150 mM NaCl, 50 mM Tris-HCl pH 7.5, 5% glycerol, 1% IGEPAL CA-630]. Cells were harvested using

trypsin/EDTA and centrifuged at 300g for 5'. Pellets were washed in PBS and then treated with RIPA lysis buffer 1x [150 mM NaCl, 50 mM Tris-HCl pH 7.5, 0.1 mM EGTA, 0,5 mM EDTA, 1% Triton X-100]. Halt Protease and Phosphatase Inhibitor Cocktail (Thermo Scientific Pierce) and Benzonase (BaseMuncher, Expedeon) were added according to the manufacturer's instructions. Protein content was determined using Bradford reagent (Bio-Rad). Extracts were mixed with NuPAGE LDS Sample Buffer and separated by SDS-PAGE. For performing the SDS-PAGE electrophoresis, lysates were loaded and run in NuPAGE Bis-Tris Gels in NuPAGE MOPS SDS Running Buffer (Thermofisher Scientific). Protein blot transfers were performed using Trans-Blot Turbo Transfer System (Biorad). Nitrocellulose blots were incubated at room temperature for 30' in blocking buffer [Tris-buffered saline with 0.1% Tween containing 5% non-fat dried milk] and then incubated overnight at 4°C in the same blocking solution with the corresponding antibodies. After washing three times for 15' each with Tris-buffered saline containing 0.1% Tween, the blots were incubated with horseradish peroxidase-conjugated (HRP) IgG, followed by washing. Immunoreactive bands were detected using the SuperSignal West Pico PLUS Chemiluminescent Substrate (Thermofisher Scientific). Developed CL-XPosure films (Thermofisher Scientific) were scanned using a flat-bed scanner and the density of the bands was measured using Gel Analyzer plugin in ImageJ software. Primary antibodies used: Anti-Ptc (1:500, Hybridoma Bank Apa1); Anti-Ref2P (1:500, abcam 178440); Anti-Actin (1:500, Hybridoma Bank JLA20s); Anti-Ci-155-full length (1:500, Hybridoma Bank 2A1); Anti-Caspase-9 (C9) (1:1000, Cell Signalling 9508); Anti-β-Actin−Peroxidase (1:20000, Sigma A3854), Anti SQSTM1 / P62 antibody (1:5000, GeneTex GTX111393).

Cell culture mammalian cells

OVCAR-3 cells were maintained in RPMI (Sigma, R8758), supplemented with 10% FBS (Life Technologies, 10500064) and grown at 37°C in a humidified atmosphere with 5% CO_2. For the experiment shown in Figure 5c and 5d, we replaced the media with fresh media containing either EtOH (0.2%) or EtOH (0.2%) + the inhibitor of autophagy bafilomycin A1 (400nM, Merck Chemicals). Cells were grown in these two different cell culture media during the last 4 hours previous the sample processing.

RNA interference

Small interfering RNA (siRNA) specific for Caspase-9 (ON-TARGETplus SMART pool human L-003309-00-0005, 842), PTCH1 (ON-TARGETplus Human PTCH1, L-003924-00-0005, 5727) and non-targeting controls (ON-TARGET plus Non-targeting Pool, D-001810-10-05) were purchased from Dharmacon Inc. (UK). Cells were plated and transfected the day after with Oligofectamine™ Transfection Reagent (Thermofisher 12252) in the presence of siRNAs according to the manufacturer's instructions. Cells were kept in the transfection mix before processing for western blot or Q-PCR at the specified time points (24h and 72h).

Gene expression analyses by Q-PCR.

RNA extraction was performed using the Qiagen RNeasy Plus kit (74034). cDNAs were synthesised with Maxima First Strand cDNA synthesis kit (Molecular Biology, Thermofisher, K1642) Q-PCR were performed using QuantiNova SYBR Green PCR Kit (Qiagen, 208054). Detection was performed using Rotor-Gene Q Real-time PCR cycler (Qiagen).

Data was analysed using the Pfaffl method, based on ΔΔ−Ct and normalised to actin as the housekeeping gene.

Gene expression was estimated with the following primers:

Patched1:

Forward CCACGACAAAGCCGACTACAT

Reverse GCTGCAGATGGTCCTTACTTTTTC

B-actin:

Forward CCTGGCACCCAGCACAAT

Reverse GGGCCGGACTCGTCATAC.

FIGURE LEGENDS:

Figure. 1 Non-apoptotic activation of initiator caspases in somatic cells of the *Drosophila* germarium.

A. Schematic drawing of the Drosophila germarium. Somatic cells relevant for this study (escort, follicular stem and follicular) are respectively depicted in green, dark blue, light blue; germline cells are shown in white.

B. Representative confocal image showing past (green channel, arrows) and present (red channel) caspase activation in ovarian somatic cells using the DBS-S-QF

sensor; TUNEL staining indicates apoptosis (gray, arrowhead); Dapi staining (blue) labels the nuclei in the entire figure. Scale bars represents 10 µm in the entire figure. Experimental flies were kept for 14 days at 29°C after eclosion and prior dissection.

C. Representative confocal image showing escort and follicular somatic cells permanently labelled with DBS-S-QF sensor (green channel, arrows); the arrowhead indicates the presence of apoptotic germline cells (rey channel, TUNEL staining, arrowhead). Notice the lack of TUNEL signal in somatic cells labelled with DBS-S-QF sensor (green). Experimental flies were kept for 14 days at 29°C after eclosion and prior dissection.

D. Graph bar indicating the percentage of ovarioles permanently labelled with DBS-S-QF sensor at 7 and 14 days; flies were raised at 18°C until eclosion, then shifted to 29°C until the indicated dissection times.

E. Schematic summarising the presumptive cells that transcribe *Dronc* at 29°C in the germarium (red).

F. Representative confocal image showing escort and follicular somatic cells in the germarium expressing Histone-RFP (red channel, arrows) under the regulation of *Dronc*$^{KO\text{-}Gal4}$ after 7 days at 29 ^{o}C; the follicular maker Castor is shown in green.

G. Biotinylation signal (green) generated in the germarium by a *Dronc*-TurboID allele; notice the signal enrichment in follicular stem cells and their progeny (white arrows) as well as the relative low levels in the germline (symbols). FasIII staining (red) labels the somatic cells and Dapi (blue) the nuclei. Experimental flies were kept for 7 days at 29°C after eclosion and prior dissection.

Figure. 2 Functional characterization of *Dronc* in somatic cells.

A-B. Confocal representative images comparing the expression of the follicular cell marker Castor in control (A: *109-30*-Gal4/+; *Dronc*^{KO} *Tub-G80*^{ts}/+, n=16) versus mutant (B: *109-30*-Gal4/+; *Dronc*^{KO} *Tub-G80*^{ts}/ UAS-*flippase Dronc*$^{KO\text{-}FRT\text{-}Dronc\text{-}GFP\text{-}APEX\text{-}FRT\text{-}QF}$, n=14) germaria. Notice the reduction in the number of Castor-expressing cells in the follicular region (white arrows). Cell nuclei labelled with Dapi (blue); Castor (green); FasIII (red). Scale bars represents 10 µm. In the entire figure, experimental flies were kept for 14 days at 29°C after eclosion and prior dissection.

C. Quantification of total number of follicular cells (left) or Castor-expressing cells (right) within the FasIII cellular domain in either heterozygous or homozygous *Dronc* mutant cells generated using the *109-30*-Gal4 and *ptc*-Gal4 drivers, respectively; the *n* number for each column in order of appearance n=16, n=14, n=20, n=17, n=19, n=18. Statistical significance was established by using unpaired parametric T-test (****p≤0.001). Median and quartiles are shown in the violin plots of the entire figure.

D-E. Representative confocal images showing Fly-FUCCI labelling in control (D: *109-30*-Gal4/FUCCI; $Dronc^{KO}$ $Tub\text{-}G80^{ts}$/+) and *Dronc* mutant (E: *109-30*-Gal4/FUCCI; $Dronc^{KO}$ $Tub\text{-}G80^{ts}$ / UAS-*flippase* $Dronc^{KO\text{-}FRT\text{-}Dronc\text{-}GFP\text{-}APEX\text{-}FRT\text{-}QF}$) follicular cells. FasIII staining (gray) is used as a reference to locate the follicular cells in the germarium; green signal labels G2, M and G1; red signal labels S, G2 and M. Notice the accumulation of cells in S-phase (red signal (arrowheads) without green (arrows) in the *Dronc* mutant condition).

F. Graph showing the relative percentage of cells in different phases of the cell cycle with germaria of the genotypes described in D and E; control (left: CTRL: n=15) versus *Dronc*-/-(right: n=16) germaria.

G. Quantification of somatic cells in S phases labelled by EdU incorporation in control (CTRL: *ptc*-Gal4/+; $Tub\text{-}G80^{ts}$/+; n=30) versus mutant (*Dronc*-/-: *ptc*-Gal4/+; $Dronc^{KO}$ $Tub\text{-}G80^{ts}$ / UAS-*flippase* $Dronc^{KO\text{-}FRT\text{-}Dronc\text{-}GFP\text{-}APEX\text{-}FRT\text{-}QF}$; n=12) germaria.

H. Quantification of total number of follicular cells (left) or Castor-expressing cells (right) within the FasIII cellular domain after manipulating the expression of several members of the caspase pathway. The genotypes and the n number of the experiments are from left to right as follows: *109-30*-Gal4/+; $Dronc^{KO}$ $Tub\text{-}G80^{ts}$ /UAS-*flippase* $Dronc^{KO\text{-}FRT\text{-}Dronc\text{-}GFP\text{-}APEX\text{-}FRT}$-suntag-Cherry-HA (n=15); *109-30*-Gal4/+; $Dronc^{KO}$ $Tub\text{-}G80^{ts}$ / UAS-*flippase* $Dronc^{KO\text{-}FRT\text{-}Dronc\text{-}GFP\text{-}APEX\text{-}FRT\text{-}Dronc}$-FLCAEA (n=14); *109-30*-Gal4/UAS-*Drice*RNAi UAS-*Decay*RNAi; $Dronc^{KO}$/UAS-*Dcp1*RNAi UAS-*Damm*RNAi (n=16); *ptc*-Gal4/UAS-*P35;* $Dronc^{KO}$ $Tub\text{-}G80^{ts}$/ UAS-*P35* (n=6). Statistical significance was established by using an ordinary one way ANOVA (n.s.= p ≥ 0.5).

Figure. 3 *Dronc* deficiency reduces Hh-signalling in *Drosophila* and OVCAR-3 ovarian somatic cells.

A-B. Representative confocal images showing the expression of Ci-155 (blue and gray channels), *ptc*-GFP (*ptc*-GFP is a *bona-fide* transcriptional read out of Hh-pathway and weak hypomorph alelle(Buszczak et al., 2007); green and gray channels) and Castor (red and gray channels) in either a control (A) or a *Dronc* mutant germaria (B). Experimental flies were kept for 14 days at 29°C after eclosion and prior dissection.

C. Quantification of *ptc*-GFP expression in either a control (n=17) or a *Dronc* mutant (n=13) germaria; unpaired parametric T-Test was used to establish the statistical significance (**** p≤0.0001). Median and quartiles are shown in the violin plots of the entire figure. Experimental flies were kept for 14 days at 29°C after eclosion and prior dissection.

D. Western blot showing Caspase-9 expression (upper lane) and actin (bottom lane, loading control) in either control or *Caspase-9* deficient OVCAR-3 cells (24h and 72h post-transfection of an shRNA against *Caspase-9*). Notice the strong downregulation of Caspase-9 at 72h.

E. mRNA levels of *patch1* measured by Q-PCR in either control or *Caspase-9* deficient OVCAR-3 cells; a Mann Whitney unpaired T-test was used to establish the statistical significance (** p≤0.01).

F-G. Castor expression (red and gray channels) in either follicular cells heterozygous (F) or homozygous (G) for *Dronc* expressing a constitutively active form of *smo* under the regulation of *109-30*-Gal4 driver. Dapi staining labels the nuclei. Experimental flies were kept for 14 days at 29°C after eclosion and prior dissection.

H. Quantification of total number of follicular cells (left) or Castor-expressing cells (right) in the following genotypes from left to right: *109-30*-Gal4/+; $Dronc^{KO}$ $Tub\text{-}G80^{ts}$ /UAS-*flippase* $Dronc^{KO\text{-}FRT\text{-}Dronc\text{-}GFP\text{-}APEX\text{-}FRT\text{-}QF}$ (n=11); *109-30*-Gal4/UAS-smo^{Act}; $Dronc^{KO}$ $Tub\text{-}G80^{ts}$/UAS-*flippase* $Dronc^{KO\text{-}FRT\text{-}Dronc\text{-}GFP\text{-}APEX\text{-}FRT\text{-}QF}$ (n=8); *109-30*-Gal4/+; $Dronc^{KO}$ $Tub\text{-}G80^{ts}$/UAS-*flippase* $Dronc^{KO\text{-}FRT\text{-}Dronc\text{-}GFP\text{-}APEX\text{-}FRT\text{-}QF}$ (n=7); *109-30*-Gal4/UAS-*Ci*; $Dronc^{KO}$ $Tub\text{-}G80^{ts}$/UAS-*flippase* $Dronc^{KO\text{-}FRT\text{-}Dronc\text{-}GFP\text{-}APEX\text{-}FRT\text{-}QF}$ (n=21). Scale bars represents 10 µm.). Statistical significance was established by using an unpaired parametric T-test (n.s.= p ≥ 0.5). Experimental flies were kept for 14 days at 29°C after eclosion and prior dissection.

I. Quantification of total number of follicular cells (left) or Castor-expressing cells (right) within the FasIII cellular domain in the following genotypes from left to right: *ptc*- Gal4/+; Tub-*G80*^{ts} /+ (n=19); *ptc*-Gal4/+; *Dronc*^{KO} Tub-*G80*^{ts}/+ (n=23); *ptc*-Gal4/+; *Dronc*^{KO} *Tub-G80*^{ts}/UAS-*Dronc* (n=14). Scale bars represents 10 µm. Statistical significance was established by using an one-way ordinary ANOVA (n.s.= p ≥ 0.5). Experimental flies were kept for 7 days at 29°C after eclosion and prior dissection.

Figure. 4 *Dronc* modulates Hh-signalling through the fine regulation of Ptc protein levels.

A. Ptc immunostaining (gray channel) in germaria of the following genotypes: (*Dronc*^{KO} *Tub-G80*^{ts} /+); (*ptc*-Gal4/+; *Tub-G80*^{ts}/+); (*ptc*-Gal4/+; *Dronc*^{KO} *Tub-G80*^{ts} /+). Scale bars represents 10 µm. In the entire figure, experimental flies were kept for 7 days at 29°C after eclosion and prior dissection.

B. Relative number of Ptc-positive punctae per germaria of the genotypes indicated in A: (*Dronc*^{KO} *Tub-G80*^{ts} /+); (n=10); (*ptc*-Gal4/+; *Tub-G80*^{ts}/+) (n=9); (*ptc*-Gal4/+; *Dronc*^{KO} *Tub-G80*^{ts} /+). (n=10). A two-way ANOVA Tukey's multiple comparisons test was used to establish the statistical significance (*** p≤0.001). Median and quartiles are shown in the violin plots of the entire figure.

C. Western blot showing Ptc (upper lane) and actin (bottom lane, loading control) expression in ovaries of the genotypes shown in A. Notice the Ptc accumulation in double heterozygous germaria (*ptc*-Gal4/+; *Dronc*^{KO} *Tub-G80*^{ts} /+).

D. Quantification of total number of follicular cells (left) or Castor-expressing cells (right) within the FasIII cellular domain in the following genotypes from left to right: *ptc*- Gal4/+; +/+ (n=17); *ptc*-Gal4/+; *Dronc*^{KO} *Tub-G80*^{ts} /UAS-*flippase Dronc*$^{KO\text{-}FRT\text{-}Dronc\text{-}GFP\text{-}APEX\text{-}FRT\text{-}QF}$ (n=16); *ptc*-Gal4/UAS-*Ptc*-RNAi; *Dronc*^{KO} *Tub-G80*^{ts} / UAS-*flippase Dronc*$^{KO\text{-}FRT\text{-}Dronc\text{-}GFP\text{-}APEX\text{-}FRT\text{-}QF}$ (n=15). Statistical significance was established by using an ordinary one-way ANOVA (**** p≤0.0001).

Figure 5. *Dronc* differentiation phenotypes are partially linked to Ptc-induced autophagy

A. Ref2P immunostaining (gray channel) in germaria of the following genotypes: (*Dronc*^{KO} *Tub-G80*^{ts} /+); (*ptc*-Gal4/+; *Tub-G80*^{ts}/+); (*ptc*-Gal4/+; *Dronc*^{KO} *Tub-G80*^{ts} /+). Scale bars represents 10 µm. In the entire figure, experimental flies were kept at 29°C after adult eclosion and prior dissection for 7 days

B. Relative number of Ref2P-positive punctae per germaria of the genotypes indicated in A: (*Dronc*^{KO} *Tub-G80*^{ts} /+); (n=15); (*ptc*-Gal4/+; *Tub-G80*^{ts}/+); (n=16); (*ptc*-Gal4/+; *Dronc*^{KO} *Tub-G80*^{ts} /+); (n=9). an ordinary one-way ANOVA Tukey's multiple comparisons test was used to establish the statistical significance (** p≤0.01, ****p≤0.0001).

C. Western blot showing Ref2P (upper lane) and actin (bottom lane, loading control) in ovaries of the genotypes shown in A. Notice the Ref2P reduction in double heterozygous germaria (*ptc*-Gal4/+; *Dronc*^{KO} *Tub-G80*^{ts} /+) compared to the (*ptc*-Gal4/+; *Tub-G80*^{ts}/+) control.

D. Quantification of total number of follicular cells (left) or Castor-expressing cells (right) within the FasIII cellular domain in the following genotypes from left to right: *ptc*-Gal4/+; *Tub-G80*^{ts}/+ (n=19); *ptc*-Gal4/+; *Dronc*^{KO} *Tub-G80*^{ts} /UAS-*flippase* *Dronc*$^{KO\text{-}FRT\text{-}Dronc\text{-}GFP\text{-}APEX\text{-}FRT\text{-}QF}$ (n=23); *ptc*-Gal4/UAS-*Atg*-RNAi; *Dronc*^{KO} *Tub-G80*^{ts} / UAS-*flippase* *Dronc*$^{KO\text{-}FRT\text{-}Dronc\text{-}GFP\text{-}APEX\text{-}FRT\text{-}QF}$ (n=10). Statistical significance was established by using an ordinary one way ANOVA Tukey's multiple comparisons test (**** p≤0.0001, *** p≤0.001, n.s.= p ≥ 0.5).

E. Western blot showing the expression levels of the autophagy marker p62 (upper lane), Caspase-9 (middle lane) and Actin (bottom lane, loading control) in either scrambled or *Caspase-9* deficient OVCAR-3 cells; the protein levels of the different read outs were measured at 72h after siRNA treatment in cells grown during the last 4 h before sample processing in our standard cell culture conditions, in cell culture media containing EtOH (0.2%), and in cell culture media containing EtOH (0.2%) + bafilomycin A1 (400nM).

F. Quantification of p62 protein levels in the experimental conditions described in E. one sample T Wilcoxon test was used to calculate statistical significance, * p≤0.05, n≥3. Bars indicate value of the mean while error bars represent the *Standard Deviation SD*.

G. Model summarising the non-apoptotic caspase effects in ovarian somatic cells. Green and red colours indicate activation or silencing, respectively.

REFERENCES

Agathocleous, M., Locker, M., Harris, W.A., and Perron, M. (2007). A general role of hedgehog in the regulation of proliferation. Cell Cycle *6*, 156-159.

Aram, L., Yacobi-Sharon, K., and Arama, E. (2017). CDPs: caspase-dependent non-lethal cellular processes. Cell Death Differ *24*, 1307-1310.

Arthurton, L., Nahotko, D., Alonso, J., and Baena-Lopez, L.A. (2019). Non-apoptotic caspase-dependent regulation of enteroblast quiescence in Drosophila. bioRxiv.

Baena-Lopez, L.A. (2018). All about the caspase-dependent functions without cell death. Semin Cell Dev Biol.

Baena-Lopez, L.A., Alexandre, C., Mitchell, A., Pasakarnis, L., and Vincent, J.P. (2013). Accelerated homologous recombination and subsequent genome modification in Drosophila. Development *140*, 4818-4825.

Baena-Lopez, L.A., Arthurton, L., Bischoff, M., Vincent, J.P., Alexandre, C., and McGregor, R. (2018). Novel initiator caspase reporters uncover previously unknown features of caspase-activating cells. Development *145*.

Bell, R.A.V., and Megeney, L.A. (2017). Evolution of caspase-mediated cell death and differentiation: twins separated at birth. Cell Death Differ *24*, 1359-1368.

Bjorkoy, G., Lamark, T., Pankiv, S., Overvatn, A., Brech, A., and Johansen, T. (2009). Monitoring autophagic degradation of p62/SQSTM1. Methods Enzymol *452*, 181-197.

Brand, A.H., and Perrimon, N. (1993). Targeted gene expression as a means of altering cell fates and generating dominant phenotypes. Development *118*, 401-415.

Briscoe, J., and Therond, P.P. (2013). The mechanisms of Hedgehog signalling and its roles in development and disease. Nat Rev Mol Cell Biol *14*, 416-429.

Burgon, P.G., and Megeney, L.A. (2017). Caspase signaling, a conserved inductive cue for metazoan cell differentiation. Semin Cell Dev Biol.

Buszczak, M., Paterno, S., Lighthouse, D., Bachman, J., Planck, J., Owen, S., Skora, A.D., Nystul, T.G., Ohlstein, B., Allen, A., *et al.* (2007). The carnegie protein trap library: a versatile tool for Drosophila developmental studies. Genetics *175*, 1505-1531.

Chai, J., Yan, N., Huh, J.R., Wu, J.W., Li, W., Hay, B.A., and Shi, Y. (2003). Molecular mechanism of Reaper-Grim-Hid-mediated suppression of DIAP1-dependent Dronc ubiquitination. Nat Struct Biol *10*, 892-898.

Chang, Y.C., Jang, A.C., Lin, C.H., and Montell, D.J. (2013). Castor is required for Hedgehog-dependent cell-fate specification and follicle stem cell maintenance in Drosophila oogenesis. Proc Natl Acad Sci U S A *110*, E1734-1742.

Dai, W., Peterson, A., Kenney, T., Burrous, H., and Montell, D.J. (2017). Quantitative microscopy of the Drosophila ovary shows multiple niche signals specify progenitor cell fate. Nat Commun *8*, 1244.

Daish, T.J., Mills, K., and Kumar, S. (2004). Drosophila caspase DRONC is required for specific developmental cell death pathways and stress-induced apoptosis. Dev Cell *7*, 909-915.

Dick, S.A., and Megeney, L.A. (2013). Cell death proteins: an evolutionary role in cellular adaptation before the advent of apoptosis. Bioessays *35*, 974-983.

Ding, A.X., Sun, G., Argaw, Y.G., Wong, J.O., Easwaran, S., and Montell, D.J. (2016). CasExpress reveals widespread and diverse patterns of cell survival of caspase-3 activation during development in vivo. Elife *5*.

Fadeel, B., and Orrenius, S. (2005). Apoptosis: a basic biological phenomenon with wide-ranging implications in human disease. J Intern Med *258*, 479-517.
Fombonne, J., Bissey, P.A., Guix, C., Sadoul, R., Thibert, C., and Mehlen, P. (2012). Patched dependence receptor triggers apoptosis through ubiquitination of caspase-9. Proc Natl Acad Sci U S A *109*, 10510-10515.
Hartman, T.R., Strochlic, T.I., Ji, Y., Zinshteyn, D., and O'Reilly, A.M. (2013). Diet controls Drosophila follicle stem cell proliferation via Hedgehog sequestration and release. J Cell Biol *201*, 741-757.
Hay, B.A., Wolff, T., and Rubin, G.M. (1994). Expression of baculovirus P35 prevents cell death in Drosophila. Development *120*, 2121-2129.
Huang, J., and Kalderon, D. (2014). Coupling of Hedgehog and Hippo pathways promotes stem cell maintenance by stimulating proliferation. J Cell Biol *205*, 325-338.
Huang, J., Reilein, A., and Kalderon, D. (2017). Yorkie and Hedgehog independently restrict BMP production in escort cells to permit germline differentiation in the Drosophila ovary. Development *144*, 2584-2594.
Huey, R.B., Wakefield, T., Crill, W.D., and Gilchrist, G.W. (1995). Within- and between-generation effects of temperature on early fecundity of Drosophila melanogaster. Heredity (Edinb) *74 (Pt 2)*, 216-223.
Jimenez-Sanchez, M., Menzies, F.M., Chang, Y.Y., Simecek, N., Neufeld, T.P., and Rubinsztein, D.C. (2012). The Hedgehog signalling pathway regulates autophagy. Nat Commun *3*, 1200.
Kirilly, D., and Xie, T. (2007). The Drosophila ovary: an active stem cell community. Cell Res *17*, 15-25.
Laws, K.M., and Drummond-Barbosa, D. (2015). Genetic Mosaic Analysis of Stem Cell Lineages in the Drosophila Ovary. Methods Mol Biol *1328*, 57-72.
Lee, R.E., Brunette, S., Puente, L.G., and Megeney, L.A. (2010). Metacaspase Yca1 is required for clearance of insoluble protein aggregates. Proc Natl Acad Sci U S A *107*, 13348-13353.
Leulier, F., Ribeiro, P.S., Palmer, E., Tenev, T., Takahashi, K., Robertson, D., Zachariou, A., Pichaud, F., Ueda, R., and Meier, P. (2006). Systematic in vivo RNAi analysis of putative components of the Drosophila cell death machinery. Cell Death Differ *13*, 1663-1674.
Li, H., Li, J., and Feng, L. (2016). Hedgehog signaling pathway as a therapeutic target for ovarian cancer. Cancer Epidemiol *40*, 152-157.
Li, S., Li, S., Wang, B., and Jiang, J. (2018). Hedgehog reciprocally controls trafficking of Smo and Ptc through the Smurf family of E3 ubiquitin ligases. Sci Signal *11*.
Li, Y., Wang, S., Ni, H.M., Huang, H., and Ding, W.X. (2014). Autophagy in alcohol-induced multiorgan injury: mechanisms and potential therapeutic targets. Biomed Res Int *2014*, 498491.
Liang, Y.Y., Lin, X., Liang, M., Brunicardi, F.C., Ten Dijke, P., Chen, Z., Choi, K.W., and Feng, X.H. (2003). dSmurf selectively degrades DPP-activated MAD and its overexpression disrupts imaginal disc development. J Biol Chem.
Liao, X., Siu, M.K., Au, C.W., Wong, E.S., Chan, H.Y., Ip, P.P., Ngan, H.Y., and Cheung, A.N. (2009). Aberrant activation of hedgehog signaling pathway in ovarian cancers: effect on prognosis, cell invasion and differentiation. Carcinogenesis *30*, 131-140.

Losick, V.P., Morris, L.X., Fox, D.T., and Spradling, A. (2011). Drosophila stem cell niches: a decade of discovery suggests a unified view of stem cell regulation. Dev Cell *21*, 159-171.

Lu, X., Liu, S., and Kornberg, T.B. (2006). The C-terminal tail of the Hedgehog receptor Patched regulates both localization and turnover. Genes Dev *20*, 2539-2551.

Martin, D.N., and Baehrecke, E.H. (2004). Caspases function in autophagic programmed cell death in Drosophila. Development *131*, 275-284.

Mauvezin, C., and Neufeld, T.P. (2015). Bafilomycin A1 disrupts autophagic flux by inhibiting both V-ATPase-dependent acidification and Ca-P60A/SERCA-dependent autophagosome-lysosome fusion. Autophagy *11*, 1437-1438.

Mille, F., Thibert, C., Fombonne, J., Rama, N., Guix, C., Hayashi, H., Corset, V., Reed, J.C., and Mehlen, P. (2009). The Patched dependence receptor triggers apoptosis through a DRAL-caspase-9 complex. Nat Cell Biol *11*, 739-746.

Moreno, E., Basler, K., and Morata, G. (2002). Cells compete for decapentaplegic survival factor to prevent apoptosis in Drosophila wing development. Nature *416*, 755-759.

Motzny, C.K., and Holmgren, R. (1995). The Drosophila cubitus interruptus protein and its role in the wingless and hedgehog signal transduction pathways. Mech Dev *52*, 137-150.

Mukherjee, A., and Williams, D.W. (2017). More alive than dead: non-apoptotic roles for caspases in neuronal development, plasticity and disease. Cell Death Differ *24*, 1411-1421.

Muro, I., Monser, K., and Clem, R.J. (2004). Mechanism of Dronc activation in Drosophila cells. J Cell Sci *117*, 5035-5041.

Napoletano, F., Gibert, B., Yacobi-Sharon, K., Vincent, S., Favrot, C., Mehlen, P., Girard, V., Teil, M., Chatelain, G., Walter, L., *et al.* (2017). p53-dependent programmed necrosis controls germ cell homeostasis during spermatogenesis. PLoS Genet *13*, e1007024.

Nezis, I.P., Simonsen, A., Sagona, A.P., Finley, K., Gaumer, S., Contamine, D., Rusten, T.E., Stenmark, H., and Brech, A. (2008). Ref(2)P, the Drosophila melanogaster homologue of mammalian p62, is required for the formation of protein aggregates in adult brain. J Cell Biol *180*, 1065-1071.

Ouyang, Y., Petritsch, C., Wen, H., Jan, L., Jan, Y.N., and Lu, B. (2011). Dronc caspase exerts a non-apoptotic function to restrain phospho-Numb-induced ectopic neuroblast formation in Drosophila. Development *138*, 2185-2196.

Pepling, M.E. (2012). Hedgehog signaling in follicle development. Biol Reprod *86*, 173.

Ray, A., Meng, E., Reed, E., Shevde, L.A., and Rocconi, R.P. (2011). Hedgehog signaling pathway regulates the growth of ovarian cancer spheroid forming cells. Int J Oncol *39*, 797-804.

Riabinina, O., and Potter, C.J. (2016). The Q-System: A Versatile Expression System for Drosophila. Methods Mol Biol *1478*, 53-78.

Rojas-Rios, P., Chartier, A., Pierson, S., Severac, D., Dantec, C., Busseau, I., and Simonelig, M. (2015). Translational Control of Autophagy by Orb in the Drosophila Germline. Dev Cell *35*, 622-631.

Rojas-Rios, P., Guerrero, I., and Gonzalez-Reyes, A. (2012). Cytoneme-mediated delivery of hedgehog regulates the expression of bone morphogenetic proteins to maintain germline stem cells in Drosophila. PLoS Biol *10*, e1001298.

Rosales-Nieves, A.E., and Gonzalez-Reyes, A. (2014). Genetics and mechanisms of ovarian cancer: parallels between Drosophila and humans. Semin Cell Dev Biol *28*, 104-109.

Roy, S., and Ingham, P.W. (2002). Hedgehogs tryst with the cell cycle. J Cell Sci *115*, 4393-4397.

Sahai-Hernandez, P., and Nystul, T.G. (2013). A dynamic population of stromal cells contributes to the follicle stem cell niche in the Drosophila ovary. Development *140*, 4490-4498.

Schneider, C.A., Rasband, W.S., and Eliceiri, K.W. (2012). NIH Image to ImageJ: 25 years of image analysis. Nat Methods *9*, 671-675.

Shinoda, N., Hanawa, N., Chihara, T., Koto, A., and Miura, M. (2019). Dronc-independent basal executioner caspase activity sustains Drosophila imaginal tissue growth. Proc Natl Acad Sci U S A *116*, 20539-20544.

Shyamala, B.V., and Bhat, K.M. (2002). A positive role for patched-smoothened signaling in promoting cell proliferation during normal head development in Drosophila. Development *129*, 1839-1847.

Singh, T., Lee, E.H., Hartman, T.R., Ruiz-Whalen, D.M., and O'Reilly, A.M. (2018). Opposing Action of Hedgehog and Insulin Signaling Balances Proliferation and Autophagy to Determine Follicle Stem Cell Lifespan. Dev Cell *46*, 720-734 e726.

Sun, G., Guzman, E., Balasanyan, V., Conner, C.M., Wong, K., Zhou, H.R., Kosik, K.S., and Montell, D.J. (2017). A molecular signature for anastasis, recovery from the brink of apoptotic cell death. J Cell Biol *216*, 3355-3368.

Szkandera, J., Kiesslich, T., Haybaeck, J., Gerger, A., and Pichler, M. (2013). Hedgehog signaling pathway in ovarian cancer. Int J Mol Sci *14*, 1179-1196.

Tang, H.L., Tang, H.M., Fung, M.C., and Hardwick, J.M. (2015). In vivo CaspaseTracker biosensor system for detecting anastasis and non-apoptotic caspase activity. Sci Rep *5*, 9015.

Terashima, J., and Bownes, M. (2004). Translating available food into the number of eggs laid by Drosophila melanogaster. Genetics *167*, 1711-1719.

Terashima, J., Takaki, K., Sakurai, S., and Bownes, M. (2005). Nutritional status affects 20-hydroxyecdysone concentration and progression of oogenesis in Drosophila melanogaster. J Endocrinol *187*, 69-79.

Vied, C., and Kalderon, D. (2009). Hedgehog-stimulated stem cells depend on non-canonical activity of the Notch co-activator Mastermind. Development *136*, 2177-2186.

Xu, D., Wang, Y., Willecke, R., Chen, Z., Ding, T., and Bergmann, A. (2006). The effector caspases drICE and dcp-1 have partially overlapping functions in the apoptotic pathway in Drosophila. Cell Death Differ *13*, 1697-1706.

Zeng, C., Chen, T., Zhang, Y., and Chen, Q. (2017). Hedgehog signaling pathway regulates ovarian cancer invasion and migration via adhesion molecule CD24. J Cancer *8*, 786-792.

Zhang, Y., and Kalderon, D. (2001). Hedgehog acts as a somatic stem cell factor in the Drosophila ovary. Nature *410*, 599-604.

Zhou, J., Peng, X., and Mei, S. (2019). Autophagy in Ovarian Follicular Development and Atresia. Int J Biol Sci *15*, 726-737.

Zielke, N., Korzelius, J., van Straaten, M., Bender, K., Schuhknecht, G.F.P., Dutta, D., Xiang, J., and Edgar, B.A. (2014). Fly-FUCCI: A versatile tool for studying cell proliferation in complex tissues. Cell Rep *7*, 588-598.

CONTRIBUTIONS

L.A.B-L. was responsible for the initial conception of the work and original writing of the manuscript. The experimental design was elaborated by A.G and L.A.B-L. A.G was responsible for most of the experimental work. D.I. performed some experiments under the supervision of A.G. The figure preparation was made by A.G and L.A.B-L. All co-authors have provided useful criticisms and commented on the manuscript before submission.

ACKNOWLEDGEMENTS

Thanks for providing flies and reagents to; Isabel Guerrero (*ptc-GFP*; Centro de Biología Molecular); Pascal Meier (UAS-*Dronc*-RNAi, UAS-*Drice*-RNAi, UAS-*Dcp*-RNAi, UAS-*Damm*-RNAi and UAS-*Decay*-RNAi); Alex Gould (anti-Castor antibody, CRICK Institute), Masayuki Miura (*Dronc*^{TurboID} and *DrIce*^{TurboID}), the Developmental Studies Hybridoma Bank (antibodies), Addgene (pCDNA3-*connexin-GFP-Apex2* plasmid), Bloomington Stock Center (fly strains), Kyoto Stock Center (fly strains), and DGRC (wild-type cDNA of *dronc*). Thanks to Genewiz and Bestgene for making the DNA synthesis and generating transgenic flies, respectively. Thanks also to Ulrike Gruneberg, Sonia Muliyil, Xavier Franch-Marro, Jordan Raff and the caspaselab members (https://www.caspaselab.com) for the critical reading of the manuscript and valuable suggestions. This work has been supported by Cancer Research UK C49979/A17516 and the John Fell Fund from the University of Oxford 162/001. L.A.B-L. is a CRUK Career Development Fellow (C49979/A17516) and an Oriel College Hayward Fellow. A.G. is a postodoctoral fellow of CRUK (C49979/A17516).

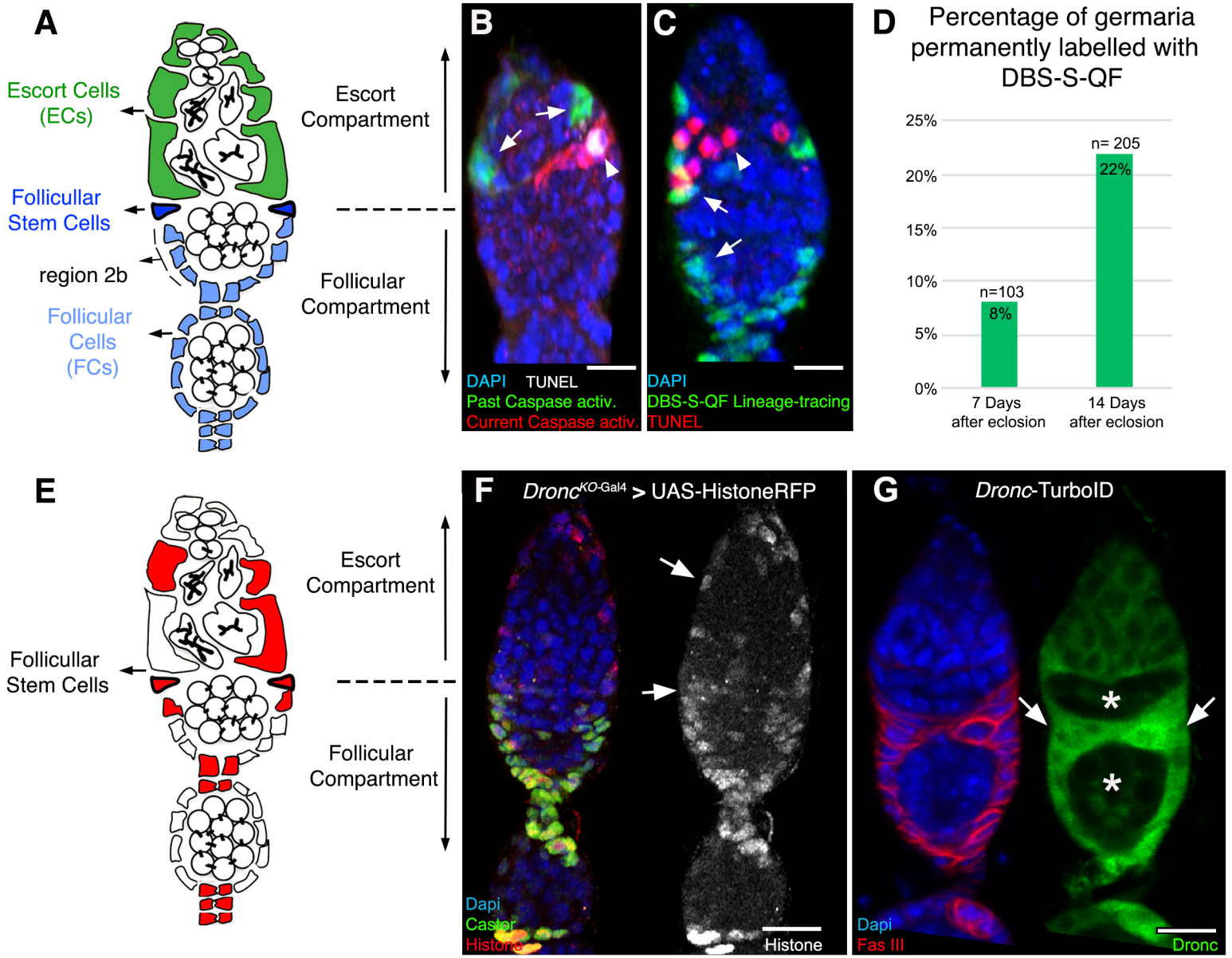

Galasso et al Figure 1

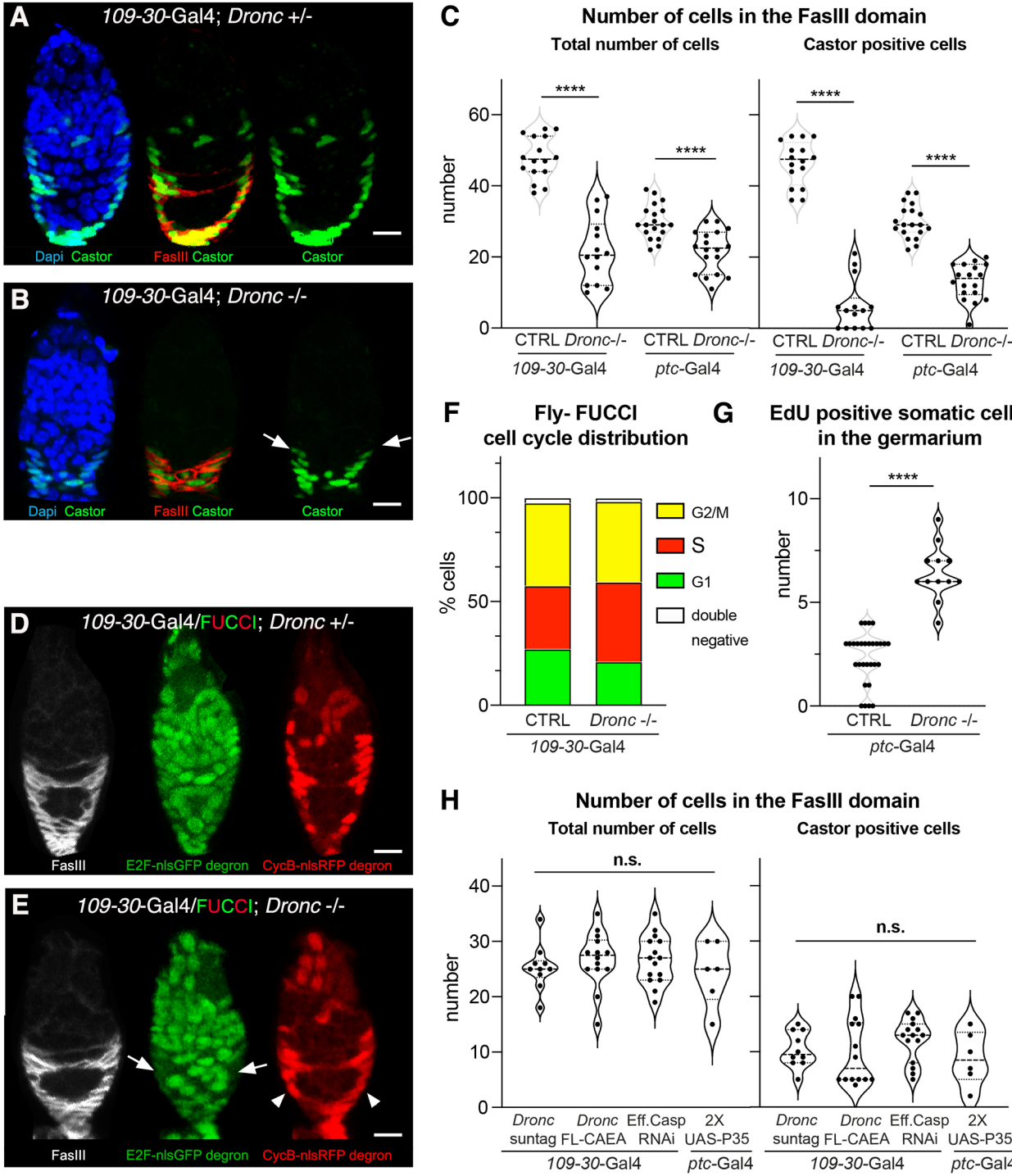

Galasso et al Figure 2

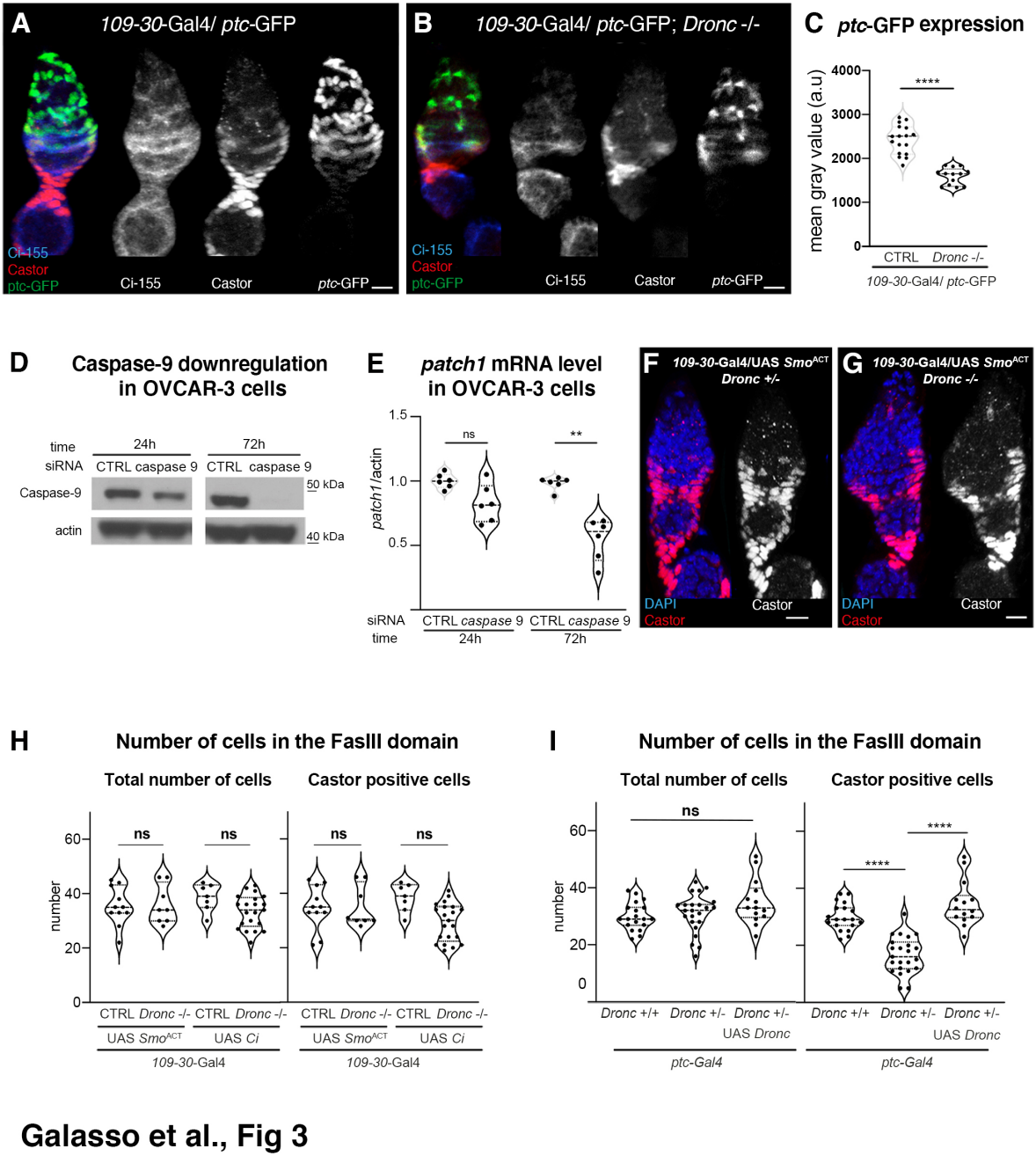

Galasso et al., Fig 3

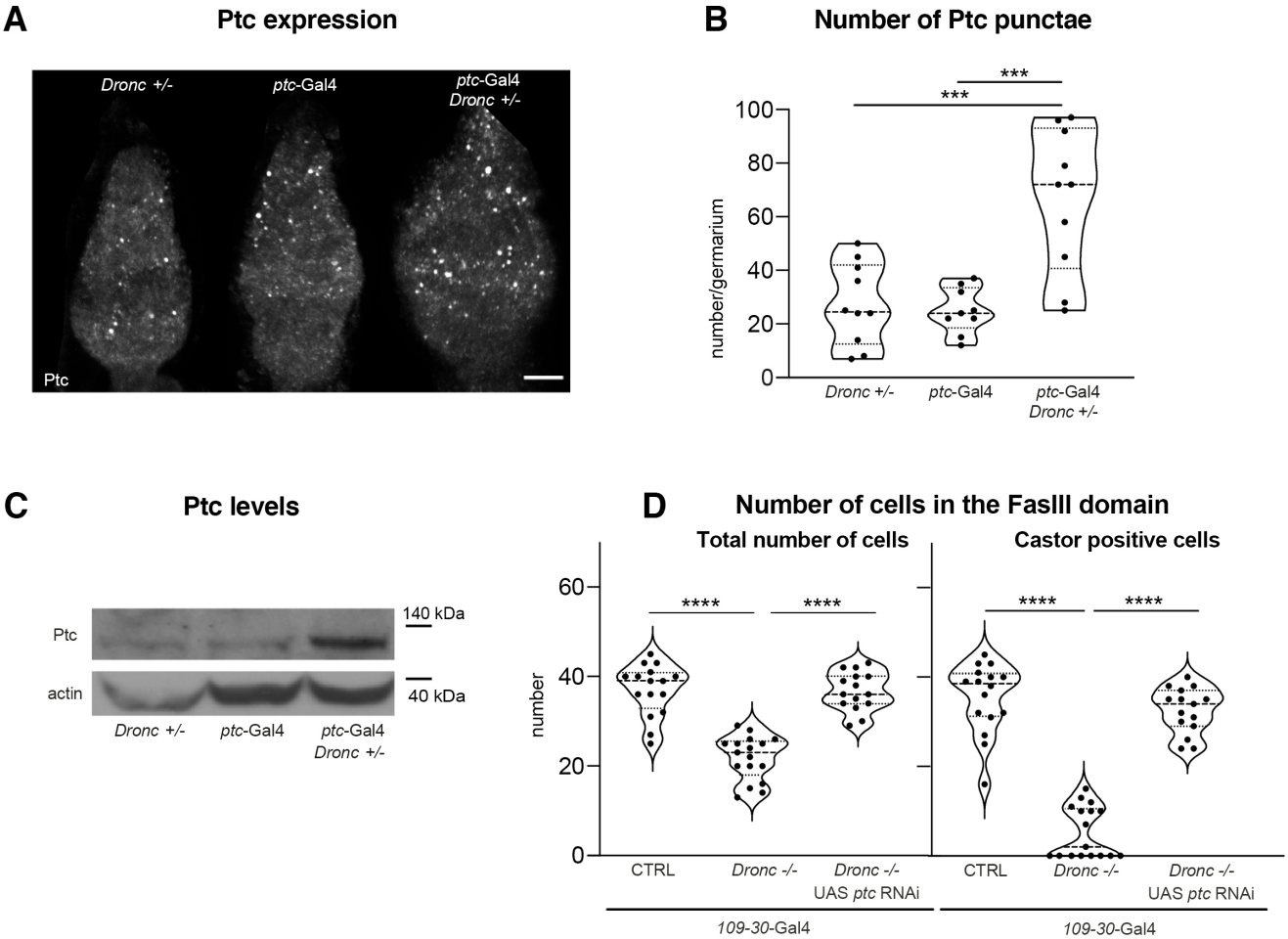

Galasso et al., Fig 4

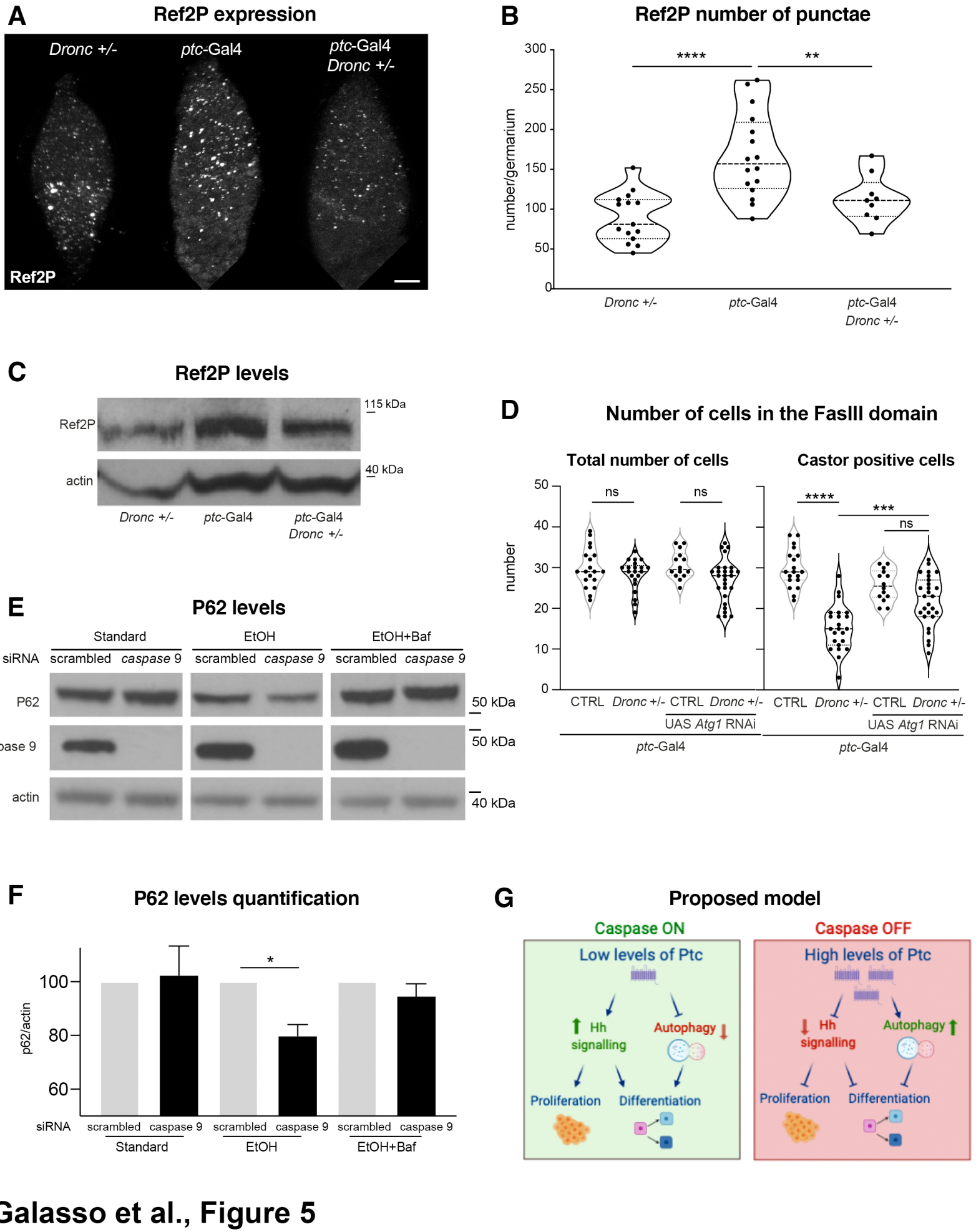

Galasso et al., Figure 5